American College *of*
Neuropsychopharmacology

ARTICLE

Check for updates

Large-scale structural network change correlates with clinical response to rTMS in depression

Sean M. Nestor[1,2], Arsalan Mir-Moghtadaei [ID]3,4, Fidel Vila-Rodriguez [ID]5, Peter Giacobbe[2,6,7], Zafiris J. Daskalakis[8], Daniel M. Blumberger[1,9,10] and Jonathan Downar [ID]1,3,4,10✉

Response to repetitive transcranial magnetic stimulation (rTMS) among individuals with major depressive disorder (MDD) varies widely. The neural mechanisms underlying rTMS are thought to involve changes in large-scale networks. Whether structural network integrity and plasticity are associated with response to rTMS therapy is unclear. Structural MRIs were acquired from a series of 70 adult healthy controls and 268 persons with MDD who participated in two arms of a large randomized, non-inferiority trial, THREE-D, comparing intermittent theta-burst stimulation to high-frequency rTMS of the left dorsolateral prefrontal cortex (DLPFC). Patients were grouped according to percentage improvement on the 17-item Hamilton Depression Rating Score at treatment completion. For the entire sample and then for each treatment arm, multivariate analyses were used to characterize structural covariance networks (SCN) from cortical gray matter thickness, volume, and surface area maps from T1-weighted MRI. The association between SCNs and clinical improvement was assessed. For both study arms, cortical thickness and volume SCNs distinguished healthy controls from MDD ($p = 0.005$); however, post-hoc analyses did not reveal a significant association between pre-treatment SCN expression and clinical improvement. We also isolated an anticorrelated SCN between the left DLPFC rTMS target site and the subgenual anterior cingulate cortex across cortical measures ($p = 0.0004$). Post-treatment change in cortical thickness SCN architecture was associated with clinical improvement in treatment responders ($p = 0.001$), but not in non-responders. Structural network changes may underpin clinical response to rTMS, and SCNs are useful for understanding the pathophysiology of depression and neural mechanisms of plasticity and response to circuit-based treatments.

INTRODUCTION

Repetitive transcranial magnetic stimulation (rTMS) is increasingly used to treat major depressive disorder (MDD) [1], as a first-line therapy [2] and in medication-resistant cases [3]. Depression has been conceptualized as a disorder involving disrupted brain network connectivity, and rTMS is thought to treat MDD by directly targeting large-scale brain systems [4–8]. Despite recent developments to shorten rTMS session duration, the intervention is time-intensive and requires daily in-clinic treatment over several weeks [9]. Understanding the network-based mechanisms that are associated with treatment response is an important step in biomarker development for rTMS in patients with MDD.

Studies of the functional network correlates of MDD have guided the development of circuit-based therapeutics. Functional imaging studies in MDD reproducibly show disconnectivity of large-scale brain networks, including the default-mode, executive control, salience and orbitofrontal networks [10–15]. Most rTMS studies have targeted the left dorsolateral prefrontal cortex

(DLPFC) in treatment-resistant depression [5, 16]. The DLPFC is a heterogenous region composed of multiple network nodes that demonstrate unique functional connectivity across several distributed brain regions including deep limbic structures such as the subgenual anterior cingulate cortex (sgACC) that are implicated in depression [7, 17–20]. Previous work also demonstrates that functional connectivity between the left DLPFC and SCC predicts response to rTMS treatment, and normalizes after treatment [5, 7, 21, 22].

Beyond functional network disruption, emerging evidence suggests that large-scale structural networks are also altered in MDD [23–27]. Previous work has reported putative changes in anterior cingulate cortex gray matter volume and cortical thickness after left DLPFC rTMS [28, 29]. Whether these structural networks are associated with response to rTMS treatment, and/or are altered following rTMS treatment, remains unclear

High-resolution magnetic resonance imaging (MRI) and multivariate computing have allowed for the characterization of large-scale

[1]Department of Psychiatry, Temerty Faculty of Medicine, University of Toronto, Toronto, ON, Canada. [2]Harquail Centre for Neuromodulation, Sunnybrook Health Sciences Centre, Toronto, ON, Canada. [3]Institute of Medical Science, Faculty of Medicine, University of Toronto, Toronto, ON, Canada. [4]Krembil Research Institute and Centre for Mental Health, University Health Network, Toronto, ON, Canada. [5]Department of Psychiatry, Non-Invasive Neurostimulation Therapies Laboratory, Institute of Mental Health, The University of British Columbia, Vancouver, BC, Canada. [6]Department of Psychiatry, Faculty of Medicine, University of British Columbia, Vancouver, BC, Canada. [7]Temerty Faculty of Medicine, Institute of Medical Science, University of Toronto, Toronto, ON, Canada. [8]Department of Psychiatry, School of Medicine, University of California, San Diego Health, San Diego, CA, USA. [9]Temerty Centre for Therapeutic Brain Intervention and Campbell Family Research Institute, Centre for Addiction and Mental Health, Toronto, ON, Canada. [10]These authors contributed equally: Daniel M. Blumberger, Jonathan Downar. ✉email: jonathan.downar@utoronto.ca

brain networks based on anatomical covariance across individuals [30, 31]. Gray matter covariance systems have emerged as a distinct framework for assessing the organization of large-scale brain networks [31]. Structural covariance networks (SCN) derived from cortical thickness and volume maps reveal commonalities in brain structure amongst distributed regions that recapitulate functional network architecture [32–34], partially correspond to white matter connectivity maps [12, 32, 34] and show alterations in depression [23, 35]. Moreover, preliminary evidence suggests that gray matter covariance may differentiate rTMS responders compared to non-responders, particularly within the frontoparietal network [23]. However, to date, no large studies have been conducted to replicate these findings. In addition, changes in cortical thickness and gray matter covariance networks have been linked to neuroplastic changes during endogenous processes such as brain maturation [30, 36–38]. However, it is not yet known whether circuit-guided treatments that involve changes in brain function, such as rTMS, can also generate detectable alterations in SCNs over the course of weeks rather than years.

We aimed to assess whether SCNs were associated with clinical response to rTMS in persons who underwent an acute course of rTMS treatment for depression. We also sought to determine whether rTMS was associated with global SCN changes and/or changes to the network directly stimulated. To assess these relationships, we examined the global SCN pattern that differentiated MDD compared to healthy control (HC) (MDD cortical signature SCN) and the SCN directly associated with the left DLPFC rTMS target (DLPFC rTMS target SCN). First, we isolated cortical thickness, volume, and surface area SCNs that (i) optimally distinguished HC and patients with MDD and that (ii) covaried with thickness, volume, and surface area of the left DLPFC rTMS target. We then assessed (iii) whether pre-treatment network integrity of these systems was associated with clinical response to rTMS, and (iv) whether post-rTMS changes in SCNs derived from serial MRI were associated with clinical improvement. These analyses were also performed in two independent arms of a large randomized clinical trial of rTMS in MDD. We hypothesized that SCNs would distinguish patients from controls, and that both their pre-treatment structure and their change in network architecture over the course of treatment would show associations with clinical improvement.

MATERIALS AND METHODS
Study overview
A total of 414 patients with MDD participated in the randomized, multi-center, non-inferiority trial, THREE-D (ClinicalTrials.gov, number NCT01887782) [16], representing one of the largest rTMS clinical trials to date. Study methods have been reported elsewhere [16]. Briefly, participants were recruited after referral to tertiary psychiatry centers at three Canadian centers (Centre for Addiction and Mental Health, Toronto, ON; Toronto Western Hospital, Toronto, ON; and the University of British Columbia Hospital, Vancouver, BC). For the current study, analyses focused on neuroimaging data from the two Toronto sites, as all their patients' scans were acquired on the same MRI scanner at the Toronto Western Hospital. The primary clinical aim of THREE-D was to assess the non-inferiority of intermittent theta-burst stimulation (iTBS) versus conventional 10 Hz rTMS for the treatment of MDD. Participants were aged 18–65 years with a Mini-International Neuropsychiatric Interview-confirmed diagnosis of MDD (single or recurrent depressive episode). MRI-guided neuronavigation localized the treatment target (left DLPFC MNI152 stereotaxic coordinates [$x - 38$, $y + 44$, $z + 26$]), a site previously shown to have maximally anticorrelated functional activity with the sgACC in MDD [7]. All patients received once-daily rTMS sessions, 5 days per week, over 4–6 weeks, for a total of 20–30 sessions of rTMS; patients were randomized to receive either iTBS or 10 Hz treatment. A CONSORT diagram for the THREE-D trial was previously published [16]. A series of non-depressed, HC subjects were also recruited from the Toronto study centers. HCs were aged 18–66 years, and did not have a diagnosis of a primary mood disorder. The HC group did not undergo stimulation with rTMS and had a single MRI. HCs were excluded if they had a history of neurological disease, psychiatric disease

(including substance abuse), or cardiovascular disease including hypertension, current use of any medications that may modulate brain perfusion (including antidepressants, mood stabilizers, neuroleptics, anxiolytics, hypnotics, stimulants, anticonvulsants, antimigraine agents, cognitive enhancing agents, opioids, anti-nausea agents, or beta-blockers), contraindications to MRI, or depression scores of >8 on the Hamilton Rating Scale in Depression (HRSD-17) scale, >12 on the Beck Depression Inventory, or >12 on the Beck Anxiety Inventory. This study was approved by research ethics boards at all study sites, and all participants provided informed consent.

Clinical depression measurement
The primary outcome measure of THREE-D was the 17-item HRSD-17 [39]. The scale was administered by trained research staff at baseline, weekly during treatment, and within a week of completing the course of rTMS.

Response group definition
In the current study, we defined responders based on ≥50% percent reduction in HRSD-17 score from baseline to the end of treatment. We also performed analyses on partial responders using ≥25% change in HRSD-17 score, as previous rTMS neuroimaging studies in depression have used this definition [4, 40].

MRI acquisition and cortical thickness processing
All participants had a pre-treatment T1-weighted high-resolution MRI. Patients, but not HC, had a second scan at 1 week post treatment. For all scans, a 3D T1-weighted fast spoiled gradient-echo anatomical scan was acquired on a 3T GE Signa HDx scanner using an 8-channel phased-array head coil (TE 12 ms, TI 300 ms, flip angle 20°, 116 sagittal slices, 1.5 mm thickness, no gap, 256 × 256 matrix, 240 mm FOV). The pre-treatment images were used for MRI-guided placement of the rTMS coil to the left DLPFC [41]. The pre-treatment and post-treatment patient scans and the HC scans were used for subsequent morphometric analyses.

Freesurfer 6.0 was used to perform all cortical parcellation steps on the T1-weighted MRIs [42] (https://surfer.nmr.mgh.harvard.edu/). Thickness was computed as the shortest straight-line distance between the pial surface and the gray-white matter boundary, and transformed using a series of linear and non-linear transformations to a standardized space for vertex-based, whole-cortex thickness analyses. Freesurfer also computes surface area at the white matter surface and a measure of cortical gray matter thickness for each vertex, which can be derived by the thickness and surface area measurements. All thickness, surface area and volume measurements were smoothed using a Gaussian kernel with a FWHM of 10. The Freesurfer parcellations were performed on a cloud computing platform, SciNet at the University of Toronto.

Two raters (SMN and AM-M) completed independent quality control analyses on all T1-weighted MRIs and cortical thickness maps. Raters were blinded to demographic and clinical variables including treatment arm but not HC/MDD. MRIs were visually inspected for artifacts using a 3D viewer. MRIs with significant artifacts were excluded from the analysis. All thickness maps were automatically rendered in three dimensions using the Freesurfer QA rendering scripts. Thickness maps were rendered in three dimensions and in the coronal plane with the pial and white matter surfaces superimposed on the participant's T1 MRI. Thickness maps were rated on a three-point scale (1 = large defects on surface, 2 = minor surface defects, and 3 = near error free). All images ranked 1, which had large errors in cortical parcellation, were excluded from the final analyses (see Supplementary Fig. 1 for examples).

Seed-based cortical thickness extraction
For each participant, we extracted the average cortical thickness, cortical gray matter volume, and surface area for an ROI that was centered over the left DLPFC rTMS target site (MNI coordinates [$x - 38$, $y + 44$, $z + 26$]) transformed into Freesurfer average surface space. This was achieved using a previously published technique that nonlinearly maps MNI152 1 mm^3 asymmetric atlas (voxel) coordinates to the Freesurfer average surface map in vertex coordinates [43]. We then generated a concentric surface-based ROI on the Freesurfer average surface map anchored by the TMS target. The algorithm performed a region-growing procedure that concentrically included up to the target vertex's fourth-order, unique, nearest-neighboring vertices. Next, we extracted the median morphometric measurements from the vertices within the surface ROI for each individual's thickness, volume, and surface area maps. We validated this method against a conventional 10 mm spherical ROI/seed and found

similar results (see Supplementary Methods and Supplementary Fig. 2). Seed extraction was performed in MATLAB R2020 (MathWorks, Natick, MA).

Statistical analyses

Univariate analyses were performed with a general linear model for continuous variables and a χ^2 test for dichotomous variables to assess for differences in demographic variables between HC and MDD rTMS responder groups, using IBM SPSS, Version 22.0 (IBM Corp., Armonk, NY).

For the multivariate SCN-based analyses, all vertex-based morphometric data were transferred to a custom-built statistical processing pipeline [32] that was based on the partial least squares (PLS) platform, using code from the Rotman Research Institute, Toronto, Canada [44, 45] (Supplementary Fig. 3). PLS has been used to identify functional brain networks [44–46] and isolate SCNs from neuroimaging data [32, 34].

The PLS method has been described in detail elsewhere [44, 45, 47]. PLS is a data-driven and multivariate method that, when applied to whole-cortex (vertex-wise) data, identifies subsets of vertices that are optimally correlated/anticorrelated with each other based on a group-level contrast or the cortical thickness/volume/surface area of a seed ROI (Supplementary Fig. 3). This technique has previously been applied successfully to identify networks of brain regions that are abnormal in thickness, volume, or surface area in other clinical populations, such as patients with Alzheimer [32, 34], patients with Parkinson's disease [48], or patients with schizophrenia [49].

Here we have applied the same set of techniques in this population of MDD patients undergoing DLPFC-rTMS. First, we performed two independent PLS analyses using cross-sectional (pre-treatment) scans to identify large-scale patterns in vertex-based cortical thickness, volume and surface area data that optimally (i) covaried with the left DLPFC target region (i.e., seed-based PLS analysis) and (ii) distinguished MDD from HC (group-wise PLS analysis), respectively. Briefly, the general PLS procedure first involved computing the correlation between two matrices to generate a cross-block correlation matrix. The first matrix contained vertex-wise cortical thickness, volume or surface area maps by individual (excluding the DLPFC seed region). The second matrix either consisted of the corresponding morphometric measurement (cortical thickness, volume or surface area) of the left DLPFC region (seed) by individual for the seed-based analysis, or else consisted of a contrast matrix of individual by group (HC/MDD) for the group-wise analysis. Each matrix was centered and normalized. For the seed-based and group-wise PLS analyses, the correlation between the two data matrices was computed and the resultant cross-block correlation matrix was submitted to a singular value decomposition. The result of the decomposition was a set of mutually orthogonal latent variables (LV) that was represented by vertex-wise weighted maps (saliences or SCNs) that optimally explained the greatest covariance (expressed as a singular value) with thickness, volume, or surface area of the left DLPFC target and the remaining cortical vertices across individuals (seed-based analyses) or thickness, volume, or surface area of brain regions that optimally distinguished HC from MDD participants (group-wise analyses).

Significance testing for PLS LVs was performed using a permutation test that randomly reordered the subjects for one of the data matrices and then recalculated the singular value decomposition 1000 times [44]. P values were estimated as the proportion of instances in which the singular values from the permuted sampling distribution exceeded the original (non-permuted) singular value. This test renders a composite set of p values from a single multivariate PLS analysis, which implicitly controls for type I error [44].

A bootstrap procedure was also performed that randomly sampled subjects with replacement and recalculated the singular value decomposition 500 times. This generated a sampling distribution for the cortical thickness, volume or surface area weights (saliences), and the standard error of the bootstrap salience distribution was computed at each vertex. The vertex-wise ratio of the salience to its bootstrap-estimated standard error was computed, and is called the Bootstrap Ratio (BSR). The bootstrap procedure computed how reliably a given vertex's weight contributed to the LV or SCN across subjects [44].

Next, a Network Integrity Index (NII) was derived for each individual for each SCN (group-wise SCN, or left DLPFC seed SCN) using a previously reported method [32, 34, 44]. Briefly, the NII was computed as the dot product between the group-level weighted network map and an individual cortical thickness, volume, or surface area map in Freesurfer average space. This value was then z-scored. The NII represented a composite value, reflecting the degree to which an individual's cortical thickness, volume, or surface area map resembles the group-level covariance pattern (LV),

including both correlated and anticorrelated network topology. NII values with higher magnitude effectively indicated higher network integrity [32, 34] or that an individual's brain more closely resembled the group-level network pattern.

For each SCN, we used Pearson correlations to assess whether pre-treatment NIIs correlated with post-treatment percent change in HRSD scores following a course of rTMS for each MDD response group. We also performed secondary analyses where we explored the correlation between pre-treatment NII and pre-treatment HRSD-17 score. All correlation analyses were adjusted for age and sex using a partial correlation.

For the MDD sample, we also performed a longitudinal analysis, where we computed NIIs using the post-treatment cortical thickness, volume and surface area maps and the SCN (salience) maps derived from the pre-treatment PLS analyses. The difference between the pre- and post-treatment NIIs (post-treatment NII – pre-treatment NII) was computed for each subject. For the principal analyses, we assessed whether there was an association between change in NIIs and percent improvement on the HRSD-17 following a course of rTMS, using Pearson correlation, and adjusted for sex and age using partial correlations. The original statistical analyses were performed blind to whether subjects received iTBS/10 Hz rTMS.

We also performed an out-of-sample validation analysis. PLS was used to compute the SCN map within an individual treatment arm (e.g., iTBS or 10 Hz rTMS) and used to derive NII values in the other arm (unseen dataset) and vice versa. We then repeated the correlation analyses between NII and HRSD-17 measures for each study arm independently.

For significant SCNs, we also performed exploratory analyses examining the relationship between the median cortical thickness, surface area or cortical volume of the DLPFC target ROI and post-treatment percent change in HRSD-17 score.

To examine whether permutation and/or bootstrap number altered the results, we repeated the main PLS analyses using 10,000 permutations and 5000 bootstraps for the cortical thickness analyses using the entire sample. These validation analyses were reported in the supplementary materials. We used 1000 permutations and 500 bootstraps for all secondary analyses.

To address whether the BSR maps relating the DLPFC target region to other parts of the cortex reflected underlying structural relationships and not regional differences in anatomical normalization, we performed a separate seed-based PLS analysis of the left sensorimotor cortex across all participants. We hypothesized that the motor cortex seed would principally covary with motor regions, bilaterally.

Supplementary Table 1 contains a complete index of all neuroimaging analyses. All correlations were adjusted for sex and age using partial correlation analysis. Primary analyses (Supplementary Table 1) were assessed with a false discovery rate (FDR) correction in SPSS. PLS analyses were computed in MATLAB R2020 (MathWorks, Natick, MA). Univariate analyses were performed in IBM SPSS Statistics for Windows, Version 22.0 (IBM Corp., Armonk, NY).

RESULTS

A total of 372 persons with MDD underwent randomization at the Toronto-based study sites. For the current study, 19 persons were excluded because they were subsequently found to not meet study inclusion criteria, and an additional 58 did not have post-treatment scans. From the remaining patients, 29 subjects were excluded because their scans failed the quality assurance measures described above ($n = 21$ for cross-sectional and $n = 11$ longitudinal). A total of 266 patients with MDD were thus included in the final analytical sample, of whom 133 belonged to each study arm (iTBS or 10 Hz rTMS treatment). A set of 70 HC individuals were also included (Table 1). There were no significant differences in age ($t[264] = -0.23$, $p = 0.82$) and/or sex ($x^2[1,266] = 1.6$, $p = 0.211$) between study arms when pooling all MDD subjects. Non-responder subgroups were significantly older for the iTBS versus the 10 Hz arm ($t[135] = 2.1$, $p = 0.038$), but this was not the case for responders ($t[127] = -1.7$, $p = 0.088$). There were no significant differences in sex proportion between arms ($x^2[1,266] = 0.21$, $p = 0.71$) or response groups ($x^2[1,266] = 0.16$, $p = 0.69$). HCs tended to be younger than patients ($t[334] = 4.5$, $p < 0.001$) but were not significantly different in sex proportion ($x^2[1,336] = 1.6$, $p = 0.21$). The iTBS arm had 1 more year of

Table 1. Study demographic and clinical data.

	HC	MDD						
		Pooled sample			iTBS rTMS Arm		10 Hz rTMS Arm	
		All MDD	Non-responder	Responder	Non-responder	Responder	Non-responder	Responder
N	70	266	137	129	68	65	69	64
Mean age (SD; range)	36 (14;18–66)	43 (12; 18–64)	42 (11; 18–62)	45 (11; 21–64)	43 (9; 19–59)	43 (11; 21–63)	40 (13; 18–62)	47 (11; 22–64)
Sex (f/m)	37/33	163/103	82/55	81/48	45/23	41/24	37/32	40/24
Mean years of education (SD)	–	17 (3)	17 (4)	16 (3)	17 (4)	17 (3)	16 (4)	16 (3)
Mean baseline HSRD-17 score (SD)	–	23 (4)	23 (4)	24 (4)	23 (4)	24 (4)	23 (5)	24 (4)
Mean %HSRD-17 change from baseline (SD)[a]	–	–43% (32)	–16% (21)	–71% (11)	–14% (22)	–73% (10)	–18% (20)	–70% (11)
Receiving pharmacotherapy during treatment N (% of total) Benzodiazepine	0	87 (33)	52 (38)	35 (27)	28 (41)	19 (29)	24 (35)	16 (25)
Antidepressant	0	211 (79)	110 (80)	101 (78)	53 (78)	47 (72)	55 (80)	56 (88)

[a]Represents the % change in HSRD-17 score from baseline to the final rTMS treatment.

education on average than the 10 Hz sample ($t[264] = 2.1$, $p = 0.039$). There were no significant differences in the proportion of persons taking a benzodiazepine between treatment arms ($x^2[1,266] = 0.84$, $p = 0.36$) or response groups ($x^2[1,266] = 3.5$, $p = 0.06$). There was no significant difference in the proportion of patients taking an antidepressant between study arms ($x^2[1,266] = 3.3$, $p = 0.07$) or response groups ($x^2[1,266] = 0.31$, $p = 0.65$).

A pre-treatment structural covariance network distinguished MDD from HC

For the whole-cortex group-wise comparison between HC and pre-treatment MDD, we found a single significant PLS LV that distinguished MDD patients from HCs for thickness (permuted $p = 0.005$) and volume (permuted $p = 0.025$) but not surface area (permuted $p = 0.13$). When accounting for multiple comparisons for the primary analyses, only the cortical thickness SCN remained significant. We refer to this covariance pattern as the MDD-signature network (Fig. 1), which co-localized to functional network regions of the default-mode and salience networks (Supplementary Fig. 4 and Supplementary Table 2). We then performed secondary PLS analyses, for the iTBS and 10 Hz arms compared to the HC sample, and found similar significant topographical patterns for thickness (iTBS permuted $p = 0.015$ and 10 Hz permuted $p = 0.002$), while only the iTBS group showed a significant SCN for volume (permuted $p = 0.023$) (Supplementary Figs. 1–8). Sensitivity analyses did not reveal significant differences in NII for participants that received either 4 or 6 weeks of treatment. Increasing the number of permutations and bootstraps by an order of 10 did not alter SCN topography (Supplementary Fig. 9). Only significant networks emerging from this analysis were submitted for further correlation analyses below.

Structural integrity and post-treatment change of the MDD-signature SCN was not associated with post-treatment clinical improvement

When pooling across treatment arms, individuals with lower baseline NII of the MDD cortical thickness signature showed a greater subsequent degree of improvement in HRSD-17 score following treatment ($r[264] = 0.13$, $p = 0.039$), but this relationship did not survive after including age and sex as covariates ($r[262] = -0.08$, $p = 0.2$). There was no significant association found for gray matter volume ($r[264] = 0.088$, $p = 0.148$).

There were no significant longitudinal relationships detected between HRSD-17 percent change and post-treatment NII percent change for the MDD-signature network across structural measures.

Cortical thickness of the left DLPFC rTMS target positively covaried with a large-scale network involving multiple distributed brain regions and negatively covaried with the sgACC cortex

When pooling across all subjects (MDD and HC), cortical thickness, volume and surface area of the left DLPFC rTMS target region each revealed a significant PLS LV (cortical thickness permuted $p = 0.0001$, volume $p = 0.001$, and surface area $p = 0.001$), which we referred to as the DLPFC target SCN. For each morphometric measure, this corresponded to a large-scale network that positively covaried with the rTMS target region, involving the cingulate and frontal cortex (Fig. 2). For the thickness SCN, the left DLPFC target region was also anticorrelated with the sgACC. We found similar results for secondary analyses of each treatment arm for thickness (iTBS permuted $p = 0.001$, 10 Hz permuted $p = 0.004$), volume (iTBS permuted $p = 0.001$, 10 Hz permuted $p = 0.001$) and surface area measures (iTBS permuted $p = 0.001$, 10 Hz permuted $p = 0.001$) (Supplementary Figs. 10–12). These results remained significant after FDR correction for multiple comparisons. We found a similar network pattern when a spherical 10 mm

PLS MDD cortical signatures

Cortical Thickness SCN

Volume SCN
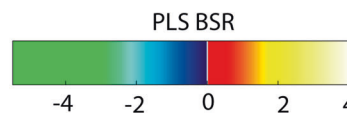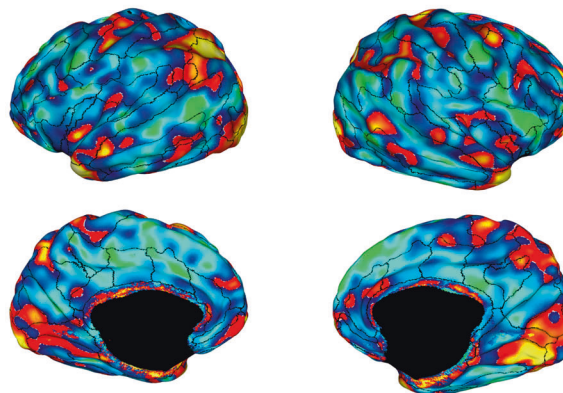

PLS BSR

-4   -2   0   2   4
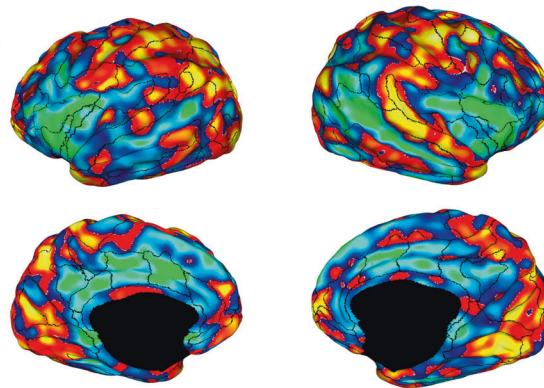
Fig. 1   A PLS-derived structural covariance network (SCN) of cortical regions that significantly and reliably distinguished persons with MDD from HC for cortical thickness (top panel) and gray matter volume (bottom panel), and consistently involved the anterior insula, medial prefrontal cortex, anterior and posterior cingulate gyrus, DLPFC cortex, and lateral temporal lobe (superior temporal sulcus). Brighter colored regions (green and yellow) represent regions that robustly contributed to the network patterns. Vertices that had Bootstrap Ratio (BSR) values with large magnitudes reflected a large contribution to the network pattern (i.e., had a small standard error and a large weight/salience) that was stable across subjects. Superimposed ROIs are derived from the Freesurfer Destrieux atlas [64].

ROI projection was used as the target seed (permuted $p = 0.0004$) (Supplementary Fig. 13) and when using 1K permutations and 500 bootstraps ($p = 0.001$) (Supplementary Fig. 14).

We also performed exploratory seed-based PLS analyses in the MDD and HC groups, individually, and we recapitulated this PLS network in the MDD group (permuted $p = 0.0001$) but not in controls (permuted p value $= 0.338$) (Supplementary Fig. 15). There were no significant differences found between treatment arms and/or controls for pre-treatment NII.

Pre-treatment NII for the DLPFC rTMS target SCN was not associated with clinical improvement
Pre-treatment NIIs were not associated with post-treatment change on the HRSD-17 across morphometric measures (thickness $r[264] = -0.088$, $p = 0.152$; surface area $r[264] = 0.047$, $p = 0.446$; volume $r[264] = 0.097$, $p = 0.114$). Exploratory analyses revealed that pre-treatment NIIs for the volume and surface area DLPFC target SCNs were correlated with pre-treatment HRSD-17 score (volume $r[262] = 0.14$, $p = 0.022$; surface area $r[262] = 0.14$, $p = 0.026$), but not thickness ($r[262] = 0.6$, $p = 0.36$).

Change in the integrity of the DLPFC target network was associated with clinical improvement in MDD rTMS responders after 6 weeks
Percent change in HRSD-17 from baseline was bimodally distributed (Supplementary Fig. 16). We examined the linear relationship between clinical response and post-treatment change in SCNs for each response group (Fig. 3). Among rTMS responders, change in NII of the DLPFC target thickness SCN was positively correlated with percent change in HRSD-17 score ($r[125] = 0.29$, $p = 0.001$) at the study endpoint. We did not find any significant relationships for surface area or volume derived NIIs, and there were no significant relationships found for change in network measures for non-responders across volumetric measures. These results also remained significant after adjusting for age and sex and applying FDR correction across responders ($r[125] = 0.28$, $p = 0.002$), Sensitivity analyses revealed that these results remained significant in responders when looking at partial responders (25% decrease from baseline HRSD-17, $r[171] = 0.18$, $p = 0.019$), and when the MDD group alone was used to generate the PLS SCN and corresponding NIIs ($r[125] = 0.27$, $p = 0.002$) (Supplementary
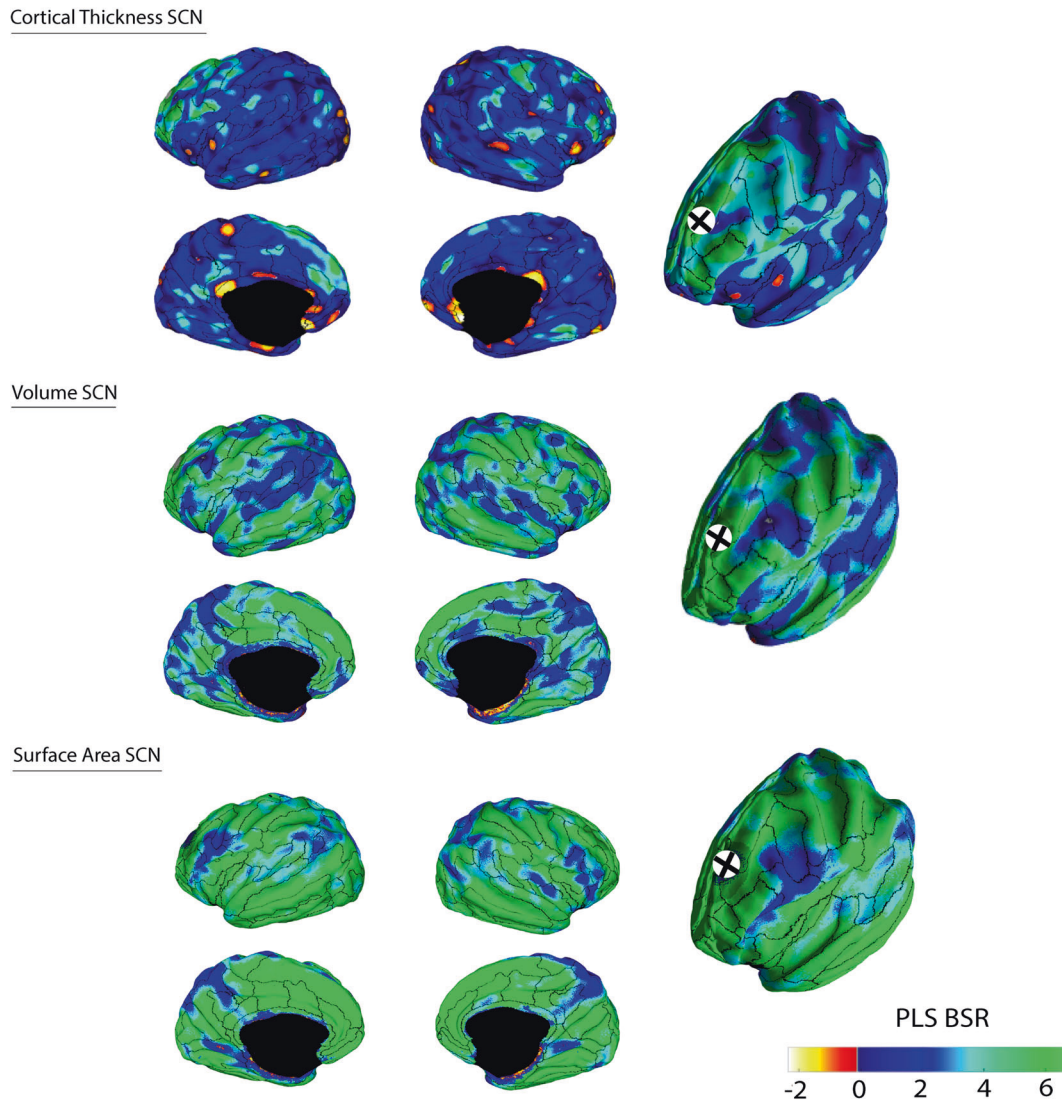
PLS Left DLPFC rTMS Target SCN

Fig. 2 **A PLS-derived structural covariance network (SCN) that corresponded to the covariance between cortical thickness, volume, or surface area of the left DLPFC rTMS target site (black cross) and the remaining cortex.** Brighter colored green or yellow regions represented regions that positively or negatively covaried with the TMS target site, respectively. Vertices that had Bootstrap Ratio (BSR) values with large magnitudes reflected a large contribution to the network pattern (i.e., had a small standard error and a large weight/salience) that was stable across subjects. Superimposed ROIs are derived from the Freesurfer Destrieux atlas [64].

Fig. 17). We also found similar results in responders when using a spherical ROI ($r[125] = 0.27$, $p = 0.002$) (Supplementary Fig. 18) or when using only 1K permutations/500 bootstraps ($r[125] = 0.27$, $p = 0.002$) (Supplementary Fig. 19).

We additionally performed out-of-sample validation analyses where we derived the DLPFC target SCN in the 10 Hz group and used this SCN map to compute NIIs for the iTBS group and vice versa. We found a similar relationship between post-treatment HRSD-17 percent change and NII change in iTBS responders ($r[61] = 0.39$, $p = 0.002$) but not 10 Hz responders ($r[60] = 0.2$, $p = 0.115$) (Fig. 3). No significant relationships were found for non-responders across modalities.

We also explored whether average pre-treatment and post-treatment change in cortical thickness, surface area and cortical volume of the DLPFC rTMS target (seed) region were associated with post-treatment percent change in HRSD-17 score across treatment arms. There were no significant relationships found across morphometric measures.

Finally, we performed a PLS seed-based validation analysis where we seeded the left motor cortex. The seed region within the left primary motor cortex covaried with regions of the bilateral motor network (permuted $p = 0.001$) (Supplementary Fig. 20)

DISCUSSION

To our knowledge, this represents one of the largest studies to date examining SCNs in MDD and the largest study to evaluate the relationship between SCNs and response to acute treatment with rTMS in MDD. This was also the first study, to our knowledge, to assess whether SCNs change after rTMS treatment. We found that decreased post-treatment integrity or expression of the group-level DLPFC target network, but not the more global MDD-signature network, was linearly associated with clinical improvement in rTMS responders. However, there was no such relationship found for non-responders. This relationship held when analyzing the iTBS and 10 Hz rTMS treatment arms
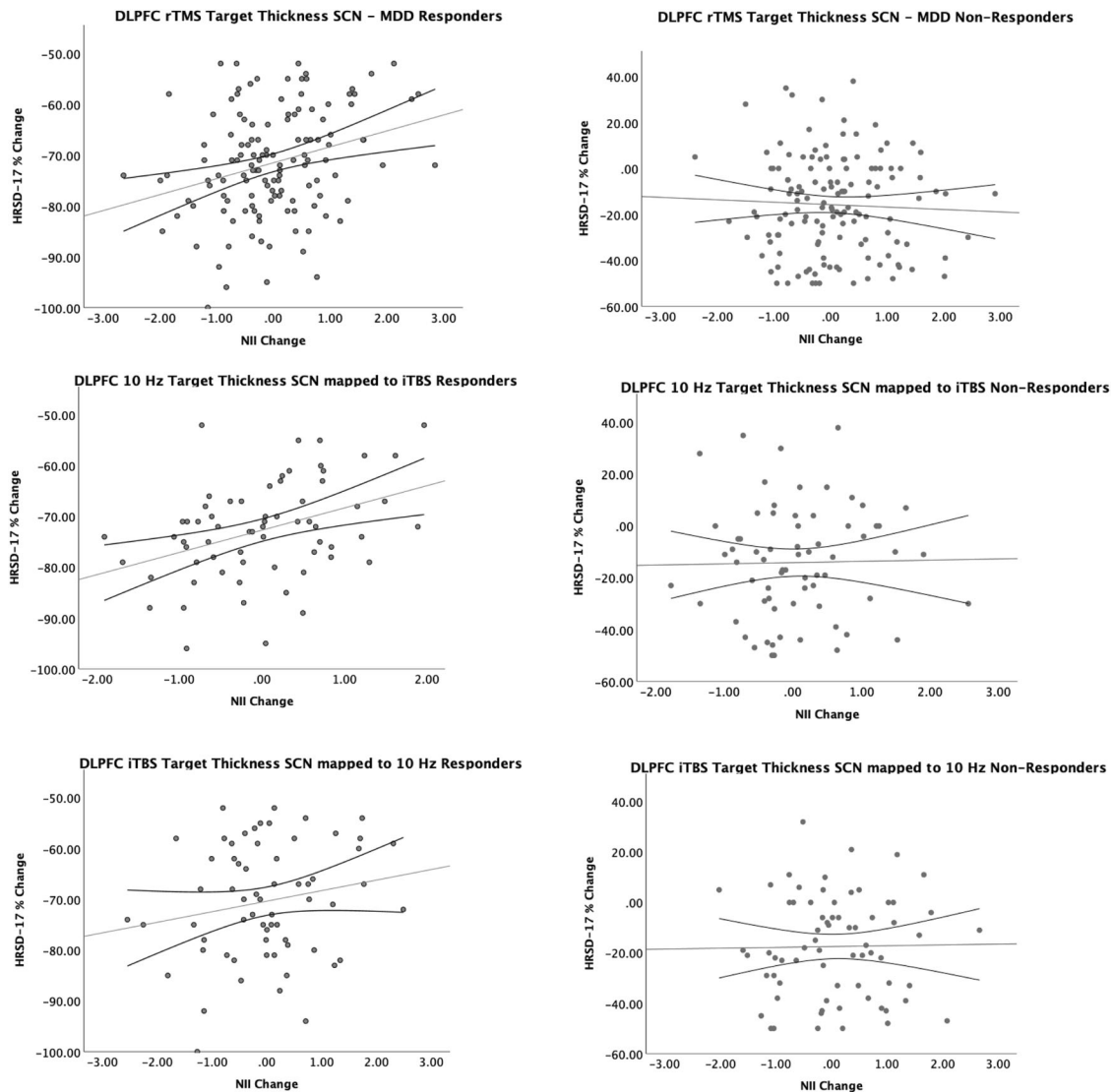
S.M. Nestor et al.

Fig. 3 Scatterplots comparing post-treatment NII change to percent change on the HRSD-17 at the study endpoint for all responders, non-responders, and treatment arm response groups. Linear trend line and 95% confidence interval were overlaid.

independently and after adjustment for sex and age. These findings suggest that post-treatment structural network changes may be specific to the network that is directly stimulated.

We isolated a global SCN that differentiated MDD from HC for cortical volume and thickness. However, neither pre-treatment structural covariance nor post-treatment change in the covariance of this SCN was associated with the clinical response after adjusting for age and sex. The MDD-signature SCN principally co-localized to functional network regions of the default-mode and salience networks. These are distributed systems of multimodal cortex that demonstrate abnormal functional connectivity in MDD and neuropsychiatric disorders [11, 13]. Intra-network regions tended to be thinner in MDD patients, aligning with previous univariate findings [50]. Others have similarly reported differences between persons with MDD and HCs in structural covariance of the salience, default-mode, executive network and medial temporal lobe systems [23, 35]. These findings are also congruent with a recent cortical thickness study, reporting altered graph-theoretical network measures in the salience and default-mode network in 76 drug-naïve patients with MDD [27].

We did not find an association between baseline SCN integrity and clinical improvement for either the global MDD-signature network or the rTMS target SCN. To our knowledge, only one other study has examined the association between structural covariance and response to rTMS in MDD, demonstrating reduced pre-treatment covariance of the executive control network in remitters ($n = 22$) compared to non-remitters ($n = 28$) and HC [23]. By contrast, the MDD-signature network in the current study excluded large portions of the DLPFC and frontoparietal network, while the left DLPFC target network failed to demonstrate a relationship between pre-treatment structural integrity and subsequent response to treatment. Methodological differences may have contributed to our divergent findings, including differences in sample size, seed-based networks of interest, morphological techniques (i.e., voxel-based versus vertex/cortical measures), interval between serial scans and multivariate platforms. It is also possible that network disruption in MDD is heterogenous. Specifically, the MDD-signature network co-localized to multiple functional systems at the group level; however, individuals may have had different networks disrupted among the default-mode, frontoparietal and salience networks that a composite NII would fail to capture.

Our DLPFC target SCN recapitulated the well-characterized anticorrelated connectivity pattern observed between the DLPFC

and sgACC in the functional MRI MDD literature [18, 51–53]. The sgACC subserves emotional processing routines and is structurally and functionally interconnected by white matter fibers with the prefrontal and limbic system, which are regions associated with depression and cognition [18, 54]. However, compared to previous functional work that found a relationship between pre-treatment functional connectivity involving the DLPFC and/or sgACC and treatment response [4, 55–59], pre-treatment structural integrity of this network was not associated with the clinical response to rTMS across morphometric measurements. Compared to the MDD group, we were not able to replicate the DLPFC rTMS target network pattern when performing a post-hoc PLS analysis in controls. It is possible that this SCN is state dependent and only exists in the context of depression versus a normal pattern of anatomical covariance in non-depressed brains. However, we did not find significant differences between HC and MDD NIIs for the pooled analysis, and the small sample of controls also limited the interpretation of these findings. Indeed, a larger sample of HCs may be required to detect this pattern, given the heterogeneity of the DLPFC [19, 20]. Future work should also compare the relationship between pre-treatment functional and structural relationships related to the DLPFC target.

Although pre-treatment DLPFC rTMS target SCN integrity was not associated with treatment response, responders demonstrated a significant positive relationship between percent reduction in HRSD-score and change in target SCN NII over the course of treatment. That is, a greater clinical response (reduction in HRSD-17 score) was associated with less expression of the pre-treatment group-level network pattern at the study endpoint. We did not find a relationship between pre-treatment rTMS target network integrity and baseline HRSD-17 score, suggesting that this finding was not driven by a regression to the mean. By contrast, we did not find any associations between clinical improvement and change in the integrity of the MDD-signature network, which overlapped with functional networks implicated in depression (default-mode and salience). This discrepancy between network findings suggests a more acute biological change to the network directly stimulated compared to more global SCN changes, that possibly change over longer intervals. However, we did not have a third MRI visit to examine these relationships.

The associations between clinical response and SCN integrity measures were modest; however, these findings provide further insight into the network-based substrates that may mediate response to rTMS, beyond traditional univariate voxel- and vertex-based morphological analyses. The linear association between clinical improvement and reduced expression of the pre-treatment DLPFC target SCN provides support for the possibility that structural network remodeling may occur over relatively short periods in patients treated with circuit-based therapies. In accordance with our findings, a previous study in forty-five patients with MDD treated with rTMS found that cortical thickness change within the sgACC was correlated with clinical improvement after 4–7 weeks of treatment [28]. A more recent study in treatment-resistant depression ($N = 31$) found no clinical improvement after four weeks of either sham stimulation or 10 Hz rTMS; however, the authors reported cortical thickening of the paralimbic cortex in the 10 Hz rTMS treated patients compared to the sham group [60]. Furthermore, an earlier study found that gray matter volume changes in the left anterior cingulate cortex were correlated with changes in the HRSD-17 after rTMS treatment in depression ($N = 27$) [29]. Others have also found increased gray matter volume in regions directly stimulated by rTMS and the corresponding contralateral homologous regions, compared to sham treatment after 5 days from baseline [61].

The potential mechanisms for rTMS induced structural changes are not yet well characterized but may involve changes in spine density [36, 61, 62]. Changes in blood flow may also mediate structural changes, as normalization of DLPFC-sgACC connectivity measured by BOLD MRI has been demonstrated following rTMS treatment [21, 57], while metabolic changes in the DLPFC metabolism have been described following antidepressant treatment [63] and deep brain stimulation [18] in similar regions to the rTMS target network identified in the current study.

We did not directly investigate the relationship between blood flow and clinical response in the current study. While it is possible that local blood flow changes within the DLPFC target site may underpin clinical response to rTMS, we did not find a relationship between post-treatment change in DLPFC target thickness and post-treatment clinical response. This may suggest a network versus local target site effect.

Limitations
In addition to the above-mentioned limitations, the THREE-D study recruited subjects from tertiary centers, with previous failed antidepressant treatment trials, and excluded persons <18 and >65 years old; these factors may limit generalization to the broader population of patients with MDD. However, our data are more reflective of a typical rTMS treatment population, as most persons receiving rTMS are also concurrently treated on a stable regimen of antidepressant medication. In addition, the HC sample was relatively smaller in size compared to the MDD sample, tended to be younger in age and had more female than male participants, which may have biased the analyses.

Although the THREE-D study demonstrated the non-inferiority of iTBS compared to 10 Hz rTMS [16], and treatment arms were matched for age, sex, and previous antidepressant treatment, we found that post-treatment change of the DLPFC target SCN did not correlate, but demonstrated a trend, with post-treatment clinical response in the 10 Hz group compared to the iTBS rTMS arm. This raises the possibility that these differing rTMS modalities may exert disparate downstream effects.

Since the analyses were performed in a common atlas space, it is possible that registration errors could also have affected the accuracy of the final results. Furthermore, the PLS analyses were data driven and could lead to false-positive results. However, we found similar results to the main analyses when computing NIIs using the network map derived from the opposite treatment arm and vice versa. Future work should prospectively validate the behavior of these SCNs across other somatic and non-somatic treatment modalities, and across a broader population of patients.

CONCLUSION
Using one of the largest rTMS datasets acquired in MDD, we found evidence that SCNs show alterations over the course of treatment that are linearly associated with clinical improvement. Our findings provide further insight into the structural mechanisms of brain plasticity following circuit-guided treatments such as rTMS.

REFERENCES
1. Lisanby SH. Noninvasive brain stimulation for depression—the devil is in the dosing. N Engl J Med. 2017;376:2593–4.
2. Milev RV, Giacobbe P, Kennedy SH, Blumberger DM, Daskalakis ZJ, Downar J, et al. Canadian Network for Mood and Anxiety Treatments (CANMAT) 2016 clinical guidelines for the management of adults with major depressive disorder. Can J Psychiatry. 2016;61:561–75.
3. Gaynes BN, Lloyd SW, Lux L, Gartlehner G, Hansen RA, Brode S, et al. Repetitive transcranial magnetic stimulation for treatment-resistant depression: a systematic review and meta-analysis. J Clin psychiatry. 2014;75:477–89. Quiz 489.
4. Cash RFH, Cocchi L, Anderson R, Rogachov A, Kucyi A, Barnett AJ, et al. A multivariate neuroimaging biomarker of individual outcome to transcranial magnetic stimulation in depression. Hum Brain Mapp. 2019;40:4618–29.
5. Cash RFH, Weigand A, Zalesky A, Siddiqi SH, Downar J, Fitzgerald PB, et al. Using brain imaging to improve spatial targeting of transcranial magnetic stimulation for depression. Biol Psychiatry. 2021;90:689–700.

6. Cash RFH, Zalesky A, Thomson RH, Tian Y, Cocchi L, Fitzgerald PB. Subgenual functional connectivity predicts antidepressant treatment response to transcranial magnetic stimulation: independent validation and evaluation of personalization. Biol Psychiat. 2019;86:e5–7.

7. Fox MD, Buckner RL, White MP, Greicius MD, Pascual-Leone A. Efficacy of transcranial magnetic stimulation targets for depression is related to intrinsic functional connectivity with the subgenual cingulate. Biol Psychiat. 2012;72:595–603.

8. George MS, Wassermann EM, Williams WA, Callahan A, Ketter TA, Basser P, et al. Daily repetitive transcranial magnetic stimulation (rTMS) improves mood in depression. Neuroreport. 1995;6:1853–6.

9. O'Reardon JP, Solvason HB, Janicak PG, Sampson S, Isenberg KE, Nahas Z, et al. Efficacy and safety of transcranial magnetic stimulation in the acute treatment of major depression: a multisite randomized controlled trial. Biol Psychiatry. 2007;62:1208–16.

10. Downar J. Orbitofrontal cortex: a 'non-rewarding' new treatment target in depression? Curr Biol. 2019;29:R59–62.

11. Downar J, Blumberger DM, Daskalakis ZJ. The neural crossroads of psychiatric illness: an emerging target for brain stimulation. Trends Cogn Sci. 2016;20:107–20.

12. Ge R, Blumberger DM, Downar J, Daskalakis ZJ, Dipinto AA, Tham JCW, et al. Abnormal functional connectivity within resting-state networks is related to rTMS-based therapy effects of treatment resistant depression: a pilot study. J Affect Disord. 2017;218:75–81.

13. Menon V. Large-scale brain networks and psychopathology: a unifying triple network model. Trends Cogn Sci. 2011;15:483–506.

14. Rao VR, Sellers KK, Wallace DL, Lee MB, Bijanzadeh M, Sani OG, et al. Direct electrical stimulation of lateral orbitofrontal cortex acutely improves mood in individuals with symptoms of depression. Curr Biol. 2018;28:3893–3902.e4.

15. Zeng L-L, Shen H, Liu L, Wang L, Li B, Fang P, et al. Identifying major depression using whole-brain functional connectivity: a multivariate pattern analysis. Brain. 2012;135:1498–507.

16. Blumberger DM, Vila-Rodriguez F, Thorpe KE, Feffer K, Noda Y, Giacobbe P, et al. Effectiveness of theta burst versus high-frequency repetitive transcranial magnetic stimulation in patients with depression (THREE-D): a randomised non-inferiority trial. Lancet. 2018;391:1683–92.

17. Padmanabhan JL, Cooke D, Joutsa J, Siddiqi SH, Ferguson M, Darby RR, et al. A human depression circuit derived from focal brain lesions. Biol Psychiat. 2019;86:749–58.

18. Mayberg HS, Lozano AM, Voon V, McNeely HE, Seminowicz D, Hamani C, et al. Deep brain stimulation for treatment-resistant depression. Neuron. 2005;45:651–60.

19. Schaefer A, Kong R, Gordon EM, Laumann TO, Zuo X-N, Holmes AJ, et al. Local-global parcellation of the human cerebral cortex from intrinsic functional connectivity MRI. Cereb Cortex. 2017;28:3095–114.

20. Gordon EM, Laumann TO, Gilmore AW, Newbold DJ, Greene DJ, Berg JJ, et al. Precision functional mapping of individual human brains. Neuron. 2017;95:791–807.e7.

21. Tik M, Hoffmann A, Sladky R, Tomova L, Hummer A, Lara LN, et al. Towards understanding rTMS mechanism of action: stimulation of the DLPFC causes network-specific increase in functional connectivity. NeuroImage. 2017;162:289–96.

22. Weigand A, Horn A, Caballero R, Cooke D, Stern AP, Taylor SF, et al. Prospective validation that subgenual connectivity predicts antidepressant efficacy of transcranial magnetic stimulation sites. Biol Psychiat. 2018;84:28–37.

23. Ge R, Downar J, Blumberger DM, Daskalakis ZJ, Lam RW, Vila-Rodriguez F. Structural network integrity of the central executive network is associated with the therapeutic effect of rTMS in treatment resistant depression. Prog Neuropsychopharmacol Biol Psychiatry. 2019;92:217–25.

24. Gong Q, He Y. Depression, neuroimaging and connectomics: a selective overview. Biol Psychiat. 2015;77:223–35.

25. Jiang X, Shen Y, Yao J, Zhang L, Xu L, Feng R, et al. Connectome analysis of functional and structural hemispheric brain networks in major depressive disorder. Transl Psychiatry. 2019;9:136.

26. Singh MK, Kesler SR, Hosseini SMH, Kelley RG, Amatya D, Hamilton JP, et al. Anomalous gray matter structural networks in major depressive disorder. Biol Psychiatry. 2013;74:777–85.

27. Wang T, Wang K, Qu H, Zhou J, Li Q, Deng Z, et al. Disorganized cortical thickness covariance network in major depressive disorder implicated by aberrant hubs in large-scale networks. Sci Rep. 2016;6:27964.

28. Boes AD, Uitermarkt BD, Albazron FM, Lan MJ, Liston C, Pascual-Leone A, et al. Rostral anterior cingulate cortex is a structural correlate of repetitive TMS treatment response in depression. Brain Stimul. 2018;11:575–81.

29. Lan MJ, Chhetry BT, Liston C, Mann JJ, Dubin M. Transcranial magnetic stimulation of left dorsolateral prefrontal cortex induces brain morphological changes in regions associated with a treatment resistant major depressive episode: an exploratory analysis. Brain Stimul. 2016;9:577–83.

30. Alexander-Bloch A, Giedd JN, Bullmore E. Imaging structural co-variance between human brain regions. Nat Publ Group. 2013;14:1–15.

31. Evans AC. Networks of anatomical covariance. NeuroImage. 2013;80:489–504.

32. Nestor SM, Mišić B, Ramirez J, Zhao J, Graham SJ, Verhoeff NPLG, et al. Small vessel disease is linked to disrupted structural network covariance in Alzheimer's disease. Alzheimer's Dement. 2017;13:749–60.

33. Seeley WW, Crawford RK, Zhou J, Miller BL, Greicius MD. Neurodegenerative diseases target large-scale human brain networks. Neuron. 2009;62:42–52.

34. Spreng RN, Turner GR. Structural covariance of the default network in healthy and pathological aging. J Neurosci. 2013;33:15226–34.

35. Watanabe K, Kakeda S, Katsuki A, Ueda I, Ikenouchi A, Yoshimura R, et al. Whole-brain structural covariance network abnormality in first-episode and drug-naïve major depressive disorder. Psychiatry Res Neuroimaging. 2020;300:111083.

36. Draganski B, Gaser C, Busch V, Schuierer G, Bogdahn U, May A. Neuroplasticity: changes in grey matter induced by training. Nature. 2004;427:311–2.

37. Ilg R, Wohlschläger AM, Gaser C, Liebau Y, Dauner R, Wöller A, et al. Gray matter increase induced by practice correlates with task-specific activation: a combined functional and morphometric magnetic resonance imaging study. J Neurosci. 2008;28:4210–5.

38. Zielinski BA, Gennatas ED, Zhou J, Seeley WW. Network-level structural covariance in the developing brain. Proc Natl Acad Sci USA. 2010;107:18191–6.

39. Hamilton M. Development of a rating scale for primary depressive illness. Br J Soc Clin Psychol. 1967;6:278–96.

40. Drysdale AT, Grosenick L, Downar J, Dunlop K, Mansouri F, Meng Y, et al. Resting-state connectivity biomarkers define neurophysiological subtypes of depression. Nat Med. 2017;23:28–38.

41. George MS, Lisanby SH, Avery D, McDonald WM, Durkalski V, Pavlicova M, et al. Daily left prefrontal transcranial magnetic stimulation therapy for major depressive disorder: a sham-controlled randomized trial. Arch Gen Psychiatry. 2010;67:507–16.

42. Fischl B. FreeSurfer. NeuroImage. 2012;62:774–81.

43. Wu J, Ngo GH, Greve D, Li J, He T, Fischl B, et al. Accurate nonlinear mapping between MNI volumetric and FreeSurfer surface coordinate systems. Hum Brain Mapp. 2018;39:3793–808.

44. McIntosh AR, Lobaugh NJ. Partial least squares analysis of neuroimaging data: applications and advances. Neuroimage. 2004;23:S250–63.

45. McIntosh AR, Bookstein FL, Haxby JV, Grady CL. Spatial pattern analysis of functional brain images using partial least squares. NeuroImage. 1996;3:143–57.

46. McIntosh AR, Mišić B. Multivariate statistical analyses for neuroimaging data. Annu Rev Psychol. 2013;64:499–525.

47. Krishnan A, Williams LJ, McIntosh AR, Abdi H. Partial least squares (PLS) methods for neuroimaging: a tutorial and review. NeuroImage. 2011;56:455–75.

48. Zeighami Y, Fereshtehnejad S-M, Dadar M, Collins DL, Postuma RB, Mišić B, et al. A clinical-anatomical signature of Parkinson's disease identified with partial least squares and magnetic resonance imaging. NeuroImage. 2019;190:69–78.

49. Kirschner M, Shafiei G, Markello RD, Makowski C, Talpalaru A, Hodzic-Santor B, et al. Latent clinical-anatomical dimensions of schizophrenia. Schizophrenia Bull. 2020;46:1426–38.

50. Schmaal L, Hibar DP, Sämann PG, Hall GB, Baune BT, Jahanshad N, et al. Cortical abnormalities in adults and adolescents with major depression based on brain scans from 20 cohorts worldwide in the ENIGMA Major Depressive Disorder Working Group. Mol Psychiatry. 2017;22:900–9.

51. Cheng W, Rolls ET, Qiu J, Liu W, Tang Y, Huang C-C, et al. Medial reward and lateral non-reward orbitofrontal cortex circuits change in opposite directions in depression. Brain. 2016;139:3296–309.

52. Mayberg HS, Liotti M, Brannan SK, McGinnis S, Mahurin RK, Jerabek PA, et al. Reciprocal limbic-cortical function and negative mood: converging PET findings in depression and normal sadness. Am J Psychiatry. 1999;156:675–82.

53. Rolls ET. A non-reward attractor theory of depression. Neurosci Biobehav Rev. 2016;68:47–58.

54. Papez JW. A proposed mechanism of emotion. 1937. J Neuropsychiatry Clin Neurosci. 1995;7:103–12.

55. Baeken C, Marinazzo D, Wu G-R, Schuerbeek PV, Mey JD, Marchetti I, et al. Accelerated HF-rTMS in treatment-resistant unipolar depression: Insights from subgenual anterior cingulate functional connectivity. World J Biol Psychiatry. 2014;15:286–97.

56. Downar J, Geraci J, Salomons TV, Dunlop K, Wheeler S, McAndrews MP, et al. Anhedonia and reward-circuit connectivity distinguish nonresponders from responders to dorsomedial prefrontal repetitive transcranial magnetic stimulation in major depression. Biol Psychiatry. 2014;76:176–85.

57. Ge R, Downar J, Blumberger DM, Daskalakis ZJ, Vila-Rodriguez F. Functional connectivity of the anterior cingulate cortex predicts treatment outcome for rTMS in treatment-resistant depression at 3-month follow-up. Brain Stimul. 2020;13:206–14.

58. Liston C, Chen AC, Zebley BD, Drysdale AT, Gordon R, Leuchter B, et al. Default mode network mechanisms of transcranial magnetic stimulation in depression. Biol Psychiat. 2014;76:517–26.

59. Salomons TV, Dunlop K, Kennedy SH, Flint A, Geraci J, Giacobbe P, et al. Resting-state cortico-thalamic-striatal connectivity predicts response to dorsomedial prefrontal rTMS in major depressive disorder. Neuropsychopharmacol. 2014;39:488–98.
60. Dalhuisen I, Ackermans E, Martens L, Mulders P, Bartholomeus J, Bruijn A, et al. Longitudinal effects of rTMS on neuroplasticity in chronic treatment-resistant depression. Eur Arch Psychiatry Clin Neurosci. 2020;65:513–9.
61. May A, Hajak G, Gänssbauer S, Steffens T, Langguth B, Kleinjung T, et al. Structural brain alterations following 5 days of intervention: dynamic aspects of neuroplasticity. Cereb Cortex. 2007;17:205–10.
62. Grutzendler J, Kasthuri N, Gan W-B. Long-term dendritic spine stability in the adult cortex. Nature. 2002;420:812–6.
63. Kennedy SH, Evans KR, Krüger S, Mayberg HS, Meyer JH, McCann S, et al. Changes in regional brain glucose metabolism measured with positron emission tomography after paroxetine treatment of major depression. Am J Psychiatry. 2001;158:899–905.
64. Destrieux C, Fischl B, Dale A, Halgren E. Automatic parcellation of human cortical gyri and sulci using standard anatomical nomenclature. NeuroImage. 2010;53:1–15.

COMPETING INTERESTS
The funder of the study (Canadian Institutes of Health Research) and the device manufacturer (MagVenture) that provided equipment had no role in study design, d-
at- a collection, data analysis, data interpretation, or writing of the report. SMN received research financial support from the Norris Scholar Award and the Labatt Family Network for Research in Depression, Department of Psychiatry, University of Toronto, and the Sunnybrook Foundation. SMN reports no conflicts of interest. AM-M reports no conflicts of interest. DMB has received research support from Brain Canada, CIHR, NIH, the Weston Brain Institute, and the Temerty Family through the CAMH Foundation and the Campbell Research Institute; he has received in-kind equipment support for investigator-initiated studies from Magventure, he has received research support and in-kind equipment support for an investigator-initiated study from Brainsway and is the site principal investigator for three sponsor-initiated studies for Brainsway; he has received medication supplies for an investigator-initiated trial from Indivior; and he has participated on an advisory board for Janssen. JD has received research support from the Arrell Family Foundation, the Buchan Family Foundation, Brain Canada, the Canadian Biomarker Integration Network in Depression, the Canadian Institutes of Health Research (CIHR), the Klarman Family Foundation, NIH, the Ontario Brain Institute, the Toronto General and Western Hospital Foundation, and the Weston Family Foundation; he has received travel stipends from Lundbeck and ANT Neuro; he has served as an advisor for BrainCheck, Neurostim TMS Centers, Restorative Brain Clinics, and TMS Neuro Solutions. FV-R has received research support from Brain Canada, the Michael Smith Foundation for Health Research, and the Vancouver Coastal Health Research Institute, and he has participated on an advisory board for Janssen. PG has received research support from the CIHR, NIH, and Veteran's Affairs Canada and has been an unpaid consultant for St. Jude Medical. He has served on an advisory board for Janssen and Bristol Myers Squibb. ZJD has received research and equipment in-kind support for an investigator-initiated study through Brainsway Inc. and Magventure Inc. His work was supported by the Ontario Mental Health Foundation (OMHF), the Canadian Institutes of Health Research (CIHR), the National Institutes of Mental Health (NIMH), and the Temerty Family and Grant Family and through the Centre for Addiction and Mental Health (CAMH) Foundation and the Campbell Institute.

ADDITIONAL INFORMATION
Supplementary information The online version contains supplementary material available at https://doi.org/10.1038/s41386-021-01256-3.

Correspondence and requests for materials should be addressed to Jonathan Downar.

Reprints and permission information is available at http://www.nature.com/reprints

Publisher's note Springer Nature remains neutral with regard to jurisdictional claims in published maps and institutional affiliations.